Ultrasound in Med. & Biol., Vol. 27, No. 12, pp. 1631–1642, 2001

0301-5629/01/$–see front matter

PII: S0301-5629(01)00451-3

● *Original Contribution*

AXIAL STRAIN IMAGING OF INTRAVASCULAR DATA: RESULTS ON POLYVINYL ALCOHOL CRYOGEL PHANTOMS AND CAROTID ARTERY

ELISABETH BRUSSEAU,* JÉRÉMIE FROMAGEAU,* GÉRARD FINET,*† PHILIPPE DELACHARTRE* and DIDIER VRAY*

*CREATIS, CNRS Research Unit (UMR 5515), INSERM; and †Department of Hemodynamics, Cardiovascular Hospital, Claude Bernard University, Lyon, France

(*Received* 27 *April* 2001; *in final form* 27 *July* 2001)

Abstract—Mapping the local elastic properties of an atherosclerotic artery is of major interest for predicting the disease evolution or an intervention outcome. These properties can be investigated by elastography, which estimates the strain distribution within a medium in response to a stress. But because diseased arteries are highly heterogeneous, a small global deformation may result in high local strains in the softest regions. For those reasons, we use in this paper the strain estimation method we recently developed to compute elastograms of original vessel-mimicking cryogel phantoms and a fresh excised human carotid artery. This adaptive method has been effectively proved to be accurate in a wider range of strains (0–7%) than commonly used gradient-based methods, and very adapted for investigating highly heterogeneous tissues. Resulting elastograms cover a wider range of strains (0–3.5%) than all previously reported intravascular elastograms, improving the discrimination between healthy and diseased regions. (E-mail: elisabeth.brusseau@creatis.insa-lyon.fr) © **2002 World Federation for Ultrasound in Medicine & Biology.**

Key Words: **Elastography, Intravascular ultrasound, Fresh excised carotid artery, Polyvinyl alcohol cryogel phantoms, Adaptive estimation, Complex cross-correlation, Phase, scaling factor, Strain.**

INTRODUCTION

Cardiovascular pathologies are one of the main causes of mortality in the Western world. Atherosclerosis, disease of the intima layer of the artery, represents the essential characteristic of arterial pathologies (Fisher et al. 2000; Zaman et al. 2000). Atherosclerosis consists of a focal accumulation of lipids, complex carbohydrates, blood cells, fibrous tissues and calcified deposits, forming a plaque that occludes progressively the lumen of the artery. When occurring within coronary arteries, the consequences of this pathology can be dramatic, like myocardial infarct, because the function of these arteries is to irrigate the cardiac muscle (Nissen et al. 1999).

The severity of a plaque results from its propensity to become complicated, the main complications being a plaque rupture, resulting in an acute thrombosis, myocardial infarction and sudden ischaemic death (Davies et al. 1985). Rupture mechanisms are complex processes correlated with plaque morphology, composition, mechanical characteristics and with the pulsatile oscillation of the blood pressure (Fung 1993; Lee et al. 1991; Lendon et al. 1991; Richardson et al. 1989). Knowledge of the local elastic properties of a plaque and of the surrounding arterial wall thus could be of fundamental interest to appreciate the vulnerability of the plaque. These properties could also provide useful information to predict the pathology evolution, as well as an intervention outcome, because procedures for curing atherosclerosis, like transluminal percutaneous angioplasty, are predominantly mechanical in nature.

Since 1960, X-ray coronary angiography is considered as the examination of reference. By providing images of the arterial profile, angiography allows the detection and the assessment of occlusion severity. But other qualitative features, like elastic properties of the plaque, cannot be revealed with this imaging technique. A more recent imaging modality, intravascular ultrasound imaging (IVUS), can be more helpful for characterising atherosclerotic lesions (Finet et al. 1997; Gussenhoven et al. 1997). Intravascular ultrasound imaging

Address correspondence to: Dr Elisabeth Brusseau, CREATIS, Batiment Blaise Pascal, 7 avenue Jean Capelle, 69621 Villeurbanne Cedex, France. E-mail: elisabeth.brusseau@creatis.insa-lyon.fr.

offers many advantages compared to classical angiography: by providing real-time high resolution cross-sectional images of the artery, this technique permits depiction of the vessel wall very precisely and atherosclerotic plaque morphology. It thus allows an accurate quantitative analysis of the disease, by precise measurements of the lumen dimensions, arterial dimensions and dimensions specific to the atherosclerotic plaque, despite being sometimes altered by inherent artefacts (Finet et al. 1993). Moreover, IVUS has the potential to characterise different plaque components (Di Mario et al. 1998; Palmer et al. 1999), but only roughly into three categories (fibrous, cell or calcified plaques) and with possible misinterpretations, which is not sufficient to predict the mechanical behaviour of the lesion. Essential complementary information is expected and might be brought by elastography, a recent imaging modality (Ophir et al. 1991) whose goal is to provide for clinicians a map of the elastic properties of any soft biological tissue (Gao et al. 1996). Based on the physical principle of elasticity, the technique consists of applying pressure on the examined medium and of estimating the induced strain distribution, by tracking the tissue motion (Hein et al. 1993, Hoeks et al. 1990, O'Donnell et al. 1994). Potential clinical applications of elastography are numerous and various, for detecting breast carcinomas (Céspedes et al. 1993, Kallel et al. 1995), prostate cancer (Lorenz et al. 1999), renal damage (Emelianov et al. 1995) or, in our case, for studying the evolution of atherosclerosis by the method of intravascular ultrasound.

Few teams have investigated intravascular elastography. Significant work has been performed by (De Korte et al 1997a) and De Korte (1999) who presented elastograms of intravascular agar-gelatine phantoms and of human femoral arteries subjected to low deformations, in the range 0–1%. They computed the axial strain distribution occurring within the arterial wall as the displacement gradient, the method assuming that the medium deformation results, within RF signals, exclusively in delays between ultrasound footprints. Commonly used gradient-based methods, whatever the time delay estimation technique applied (Konofagou et al. 1998; Lubinski et al. 1999, Xu et al. 1995), are accurate for very small deformation (0–1.5/2%) but fail rapidly with increasing strains, because they ignore the signal shape variation induced by the physical compression of the medium. It turns out that, owing to the high heterogeneous character of atherosclerotic plaque composition, the local Young's modulus can vary by several orders of magnitude (1–1000 kPa) over the investigated medium and a small global deformation might result in a high local deformation over the regions where the Young's modulus is the weakest. This makes it necessary to increase the range of validity of the previously mentioned strain estimation methods. One improvement has been to stretch the entire postcompression signal temporally by an appropriate constant factor prior to time delay estimation (Alam et al. 1997). This preprocessing has been proved to compensate fairly well for the effect of compression at low strains. However, this technique suffers from two fundamental limits: first, the value of the proper temporal stretching factor requires an *a priori* knowledge of the strain magnitude; second, this factor depends on the local deformation and cannot be constant over the signal. A similar approach in 2D also has been introduced by Chaturvedi et al. (1998) that consisted in companding the data images in the axial and lateral directions, first globally then locally, before correlation-based time-delay measurements.

In a first study, Alam *et al.* (1998) took into account the change in the shape of signals and considered the signal after compression as a locally delayed and scaled replica of the signal before deformation. The local scaling factor, directly related to the local strain, is estimated over each segment of study as the factor that maximises the correlation between the precompression and stretched postcompression signal segments. This study has shown that using local scaling factors leads to a method that is much more robust in terms of decorrelation noise.

We recently developed an adaptive strain estimation method based on the computation of local scaling factors (Brusseau et al. 2000a) via the study of the phase difference between pre- and postcompression signals. To achieve maximum accuracy, the method first selects, within the pre- and postcompression signal, segments that are representative of the same part of tissue. For each pair of signal segments, the scaling factor is then estimated by iterative variation until reaching a zero mean phase difference between the associated complex pre- and scaled postcompression signals. Its adaptability makes this method appropriate for computing scaling factors resulting from larger strains or a wide spread of strain variations and, therefore, for estimating strains in strongly heterogeneous media, like atherosclerotic arteries.

In this paper, we use the method we have developed to compute elastograms of original intravascular cryogel phantoms and of a fresh carotid artery. The materials and methods, including the signal processing method, the experimental set-up and phantoms are described in the next section. In the next section, the experimental results from the cryogel phantoms and the human carotid artery are presented, followed by a discussion and conclusions detailed in the last section.

MATERIALS AND METHODS

Experimental set-up description

Performing elastographic experiments in the intravascular case requires a specific device allowing both application of a pressure inside the lumen of the phantom

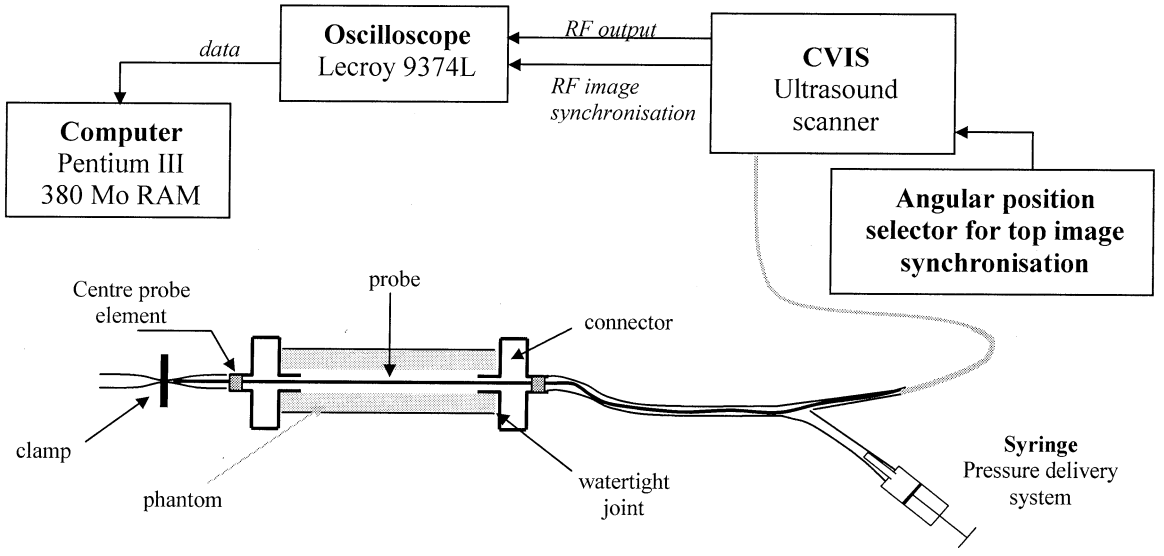

Fig. 1. Scheme of the instrumental set-up for elastographic intravascular experiments.

or of the artery under examination, and acquisition of RF data. The experimental set-up consists of a CVIS ultrasound scanner, working with a 30 to 40-MHz mechanical rotating single element, a digital oscilloscope Lecroy 9374L and a self-made pressuring system. A scheme of the experimental set-up is given in Fig. 1. The phantom is positioned between two watertight connectors, at each lateral extremity. This watertight device is equipped with sheaths at both sides. At the proximal side, the intravascular catheter is introduced through the sheath into the lumen of the phantom or the artery and then through the distal sheath. By two guiding elements, the probe is fixed approximately at the lumen centre, to limit geometrical artefacts and motion of the probe. The distal sheath is clamped to ensure the watertight character of the system. The proximal sheath is also connected to a syringe. The system composed of the distal and proximal sheaths of the artery or phantom and of the syringe is a watertight one. Because sheaths are rigid, injecting fluid inside this system results in an increase of the pressure inside the phantom or arterial lumen. Inner pressure is therefore manually increased or decreased by varying the fluid volume (precision $\Delta V = 0.01$ ml) inside the lumen. A scan of 256 angles is performed at each static pressure. Sampling of the data is phase-synchronised with the top image synchroniser (external output of the CVIS ultrasound scanner). The top image synchroniser permits the beginning of image acquisition when the ultrasound beam reaches a specific user-determined angular position, resulting in acquisition of sets of angularly aligned images. With this configuration, RF data are not acquired in an image format but in a single signal format, containing the 256 consecutive RF lines composing the image. The images are then reconstructed. RF data were digitised at a sampling frequency of 500 MHz (sample interval: 1.5 μm) in 8-bit format, stored on the 520 Mo PCMCIA hard disk in the Lecroy oscilloscope and processed off-line. Experiments were performed at room temperature on cryogel phantoms and on a human carotid artery.

Cryogel intravascular phantom description

Tissue-mimicking phantoms, commonly used for elastographic experiments, are made from a mixture of agar and gelatine. The association of agar and gelatine has effectively revealed interesting properties, because gelatine contributes to the elastic character of the resulting material, whereas agar ensures stiffness and cohesion (De Korte et al. 1997b; Hall et al. 1997). As for the acoustical scattering of such phantoms, it can be adjusted very easily by simply varying the scatterer concentration. The independent control of acoustical and mechanical properties, the facility to manage acoustically homogeneous phantoms and the resulting incompressible character of these test objects have made agar-gelatine phantoms attractive for elastographic experiments.

Although these phantoms seem to be adequate for experiments with external ultrasound, this seems different for intravascular ultrasound. Indeed, owing to the considered geometry, a hollow thin-walled cylinder subjected to an inner pressure, agar-gelatine intravascular phantoms tend to rupture easily under an increasing stress and, therefore, do not mimic the ruggedness and elasticity of arteries. For these reasons, we have used for this specific application another material, presenting a high inherent breaking strength and able to endure the

rigours of pulsatile flow and general handling (Chu et al. 1997; Surry et al. 1998). This material, never used previously for ultrasound elastographic experiments, is termed polyvinyl alcohol cryogel (PVA-C). As a cryogel, it acquires its properties by freeze-thaw processes. Chu and Rutt (1997) have studied this particular material, and found that the acoustical and elastic characteristics of the PVA cryogel are within the range of those of soft biological tissues. More precisely, although the speed of sound depends on several parameters, like PVA or acoustical particles concentrations, it remains within the physiological range (1500–1600 m/s). Initial results on sound attenuation values are also promising, being in the range of 1–3 dB/cm at 5 MHz. Dealing with the mechanical properties, this material presents an incompressible character, resulting in its 3D deformation under an applied pressure. Moreover, results from experiments lead by Chu and Rutt (1997) have shown that the stress–strain relationship of cryogel intravascular phantoms is close to that of a pig aorta. Thus, PVA-C phantoms present a mechanical behaviour similar to that of arteries, making them very suitable for performing intravascular elastography.

Axial strain estimation method description

We recently developed a signal-processing method for axial strain estimation. This method is based on the principle that the physical compression of tissues produces changes within signals comparable to local scaling factors. In a first approximation, the postcompression signal can thus be considered as a locally delayed and compressed replica of the precompression signal. Our estimation of the axial strain results from four main steps: (i) arterial wall signals extraction and registration; (ii) adaptive windowing; (iii) scaling factor estimation; and (iv) strain estimates computation.

Arterial wall signals extraction and registration. Prior to strain estimation, an extraction and registration of the beginning of the pre- and postcompressed signals relative to the arterial wall has to be performed. The use of the top image synchroniser, which performs the acquisition of angular aligned images as well as the use of anechoic physiological fluid inside the phantom or arterial lumen, highly facilitates this preprocessing. This one follows two steps. First, a global detection of the blood–wall interface is performed by a thresholding in amplitude on the corresponding envelope images. Then, a fine registration, by estimating the remaining delay between the beginning of the RF arterial wall signals at two different endoluminal pressures, is achieved by cross-correlation.

Adaptive windowing. Signal segments containing the acoustical signature of the same part of tissue before and after deformation are selected. This selection is performed by displacing the window of study on the postcompression signal in an adaptive manner (eqn 2) compared to the regular displacement of this window on the precompression signal (eqn 1). This adaptive displacement is directly related to the previous strains.

$$d_i = i\Delta \tag{1}$$

$$d'_i = d'_{i-1} + (1 - \varepsilon_{i-1})\,\Delta = \sum_{k=0}^{i-1} (1 - \varepsilon_k)\Delta \tag{2}$$

where i = number of displacement steps of the window of study in the depth direction; d_i = cumulative window displacement on the precompression signal; d'_i = cumulative window displacement on the postcompression signal [during processing, this displacement is converted to an integer sample number, introducing an error of maximum one sample (1.5 μm)]; Δ = window displacement step; and ε_i = strain value on the ith window.

Equation 2 clearly shows that the displacement is adapted at each step. The more the tissue is compressed, the higher the displacement will be. So, for no tissue deformation ($\varepsilon = 0$), the window displacement on the pre- and postcompression signal is identical and therefore the relative window displacement between the pre- and postcompressed states will be zero. Otherwise, the higher the strain, the more this relative displacement will increase.

Scaling factor estimation. Having selected two corresponding signal segments, the second step of our method is the estimation of the local compression factor α itself. It is assumed that this factor is constant over the window of study. Let us denote by $s_1(t)$ and $s_2(t)$ the signal segments containing the acoustical signature of the same region before and after the deformation ($s_1(t)$, $s_2(t)$ as issued from step (i)).

$$s_2(\alpha t) = s_2(t + (\alpha - 1)t) = s_1(t) \tag{3}$$

with α, compression factor ≤ 1.

The scaling factor is estimated by iteratively stretching the postcompression echo signal until reaching a minimal mean phase difference with the precompression echo signal. In practical terms, stretching a discrete signal s by a factor α has been performed by replacing each sample value $s(k)$ by $s(k/\alpha)$, the latter being computed by linear interpolation.

To compute the scaling factor between the two signals $s_1(t)$ and $s_2(t)$, we have defined the phase function ϕ so that:

$$\phi(\beta) = \arg\left(\frac{1}{T}\int_0^T \tilde{s}_1(t)\tilde{s}_2^*(\beta t)dt\right) \quad (4)$$

with $\tilde{s}_1$ (respectively $\tilde{s}_2$), the analytic signal associated with the RF echo signal s_1 (respectively s_2) and β the stretching factor applied to s_2. The unwrapped phase ϕ is a continuous linear and strictly monotonic function. We can observe that, when ϕ is positive, s_2 is a stretched version of s_1 when it is zero, s_2 is identical to s_1 and when ϕ is negative, s_2 is a compressed version of s_1. It is interesting to note that ϕ, for a given value of β, also represents the phase of an averaged value, which is the scalar product averaged on the time interval T. This leads to a reduction of phase fluctuations in the presence of additive noise. Finding the zero-crossing is achieved by dichotomy. This technique consists of performing a framing of a zero of a function and reducing this framing until the searched value with the desired accuracy is reached. An interval containing the zero of the function is given as the initial condition. The sign of the phase, therefore, changes on this interval. Then, the interval is iteratively reduced by keeping a sign change. This method offers the advantage of being accurate and of rapidly converging to the solution. Note that, because the unwrapped phase is a monotonic function, it is very well adapted to such processing. The estimated stretching factor β is the inverse value of the compression factor of the medium, α.

Strain estimates computation. Having estimated the scaling factor $\hat{\beta}$, the strain is then directly deduced as:

$$\hat{\varepsilon} = 1 - 1/\hat{\beta} \quad (5)$$

The method we have developed presents the characteristic of being adaptive, making it appropriate for computing scaling factors resulting from larger strains or a wide spread of strain variations and is, therefore, appropriate for investigating atherosclerotic arterial walls. Previous results from simulations and phantoms have shown that this method remains accurate for deformations up to 7%.

EXPERIMENTAL RESULTS

Experiments were performed with two types of intravascular cryogel phantoms, homogeneous (Brusseau et al. 2000b) and layered ones, and with a fresh excised human carotid artery. In this study, we have estimated the strain field generated by a variation of the endoluminal pressure and occurring in the radial direction. The variation of pressure inside the lumen was performed by increasing the fluid pressure.

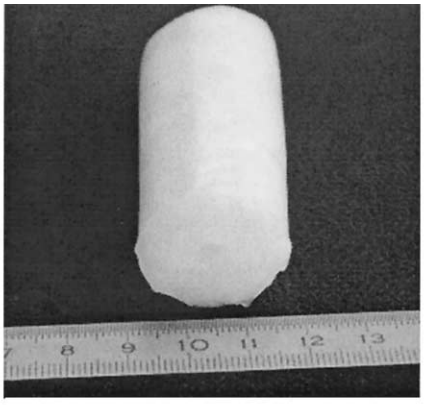

(a)

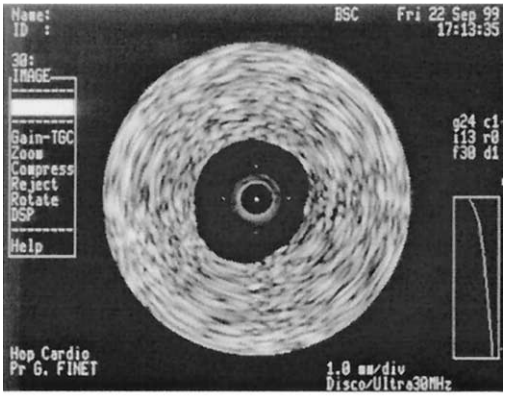

(b)

Fig. 2. Description of the homogeneous intravascular cryogel phantom. The geometrical characteristics of this phantom are a 5 mm lumen diameter, a 10 mm wall thickness and a 60 mm length. The mechanical properties of that phantom result from one freeze-thaw cycle. (a) Photograph of the phantom; (b) B-mode image of the phantom.

Results on an homogeneous phantom

The first phantom we investigate is a homogeneous (one-layer) intravascular phantom. The geometrical features of this test object are a 5-mm lumen diameter, a 10-mm wall thickness and a 60-mm length (Fig. 2a). Its mechanical characteristics result from one freeze-thaw cycle. The acoustical properties were managed during the building procedure by adding 1% of acoustical scatterers (silicon-carbide (SiC), mean diameter 15 μm). The resulting elastograms in Cartesian and polar coordinates are displayed in Fig. 3a and b, respectively. They have been computed by using a 0.25-mm window length with 80% overlap. A 5×5 median filtering was applied to the estimates, to reduce noise. Caution was taken not to erode the border values. The strain distribution results

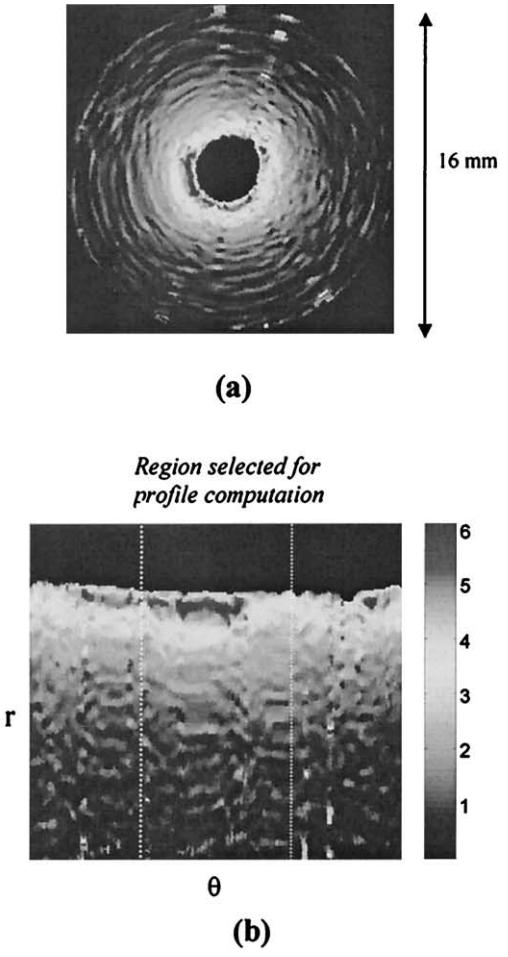

Fig. 3. Experimental result with a homogeneous intravascular cryogel phantom. (a) Resulting elastogram in Cartesian coordinates computed over a region of 8 mm depth with a 0.25 mm window length and 80% overlap; (b) elastogram in polar coordinates; and (c) mean strain profile (solid line) and curve in A/r^2 (dashed line). Although the phantom is homogeneous, the corresponding elastogram presents a decrease, which matches perfectly the $1/r^2$ model. This decrease of the strain is directly related to the loss of the stress magnitude along the wall thickness.

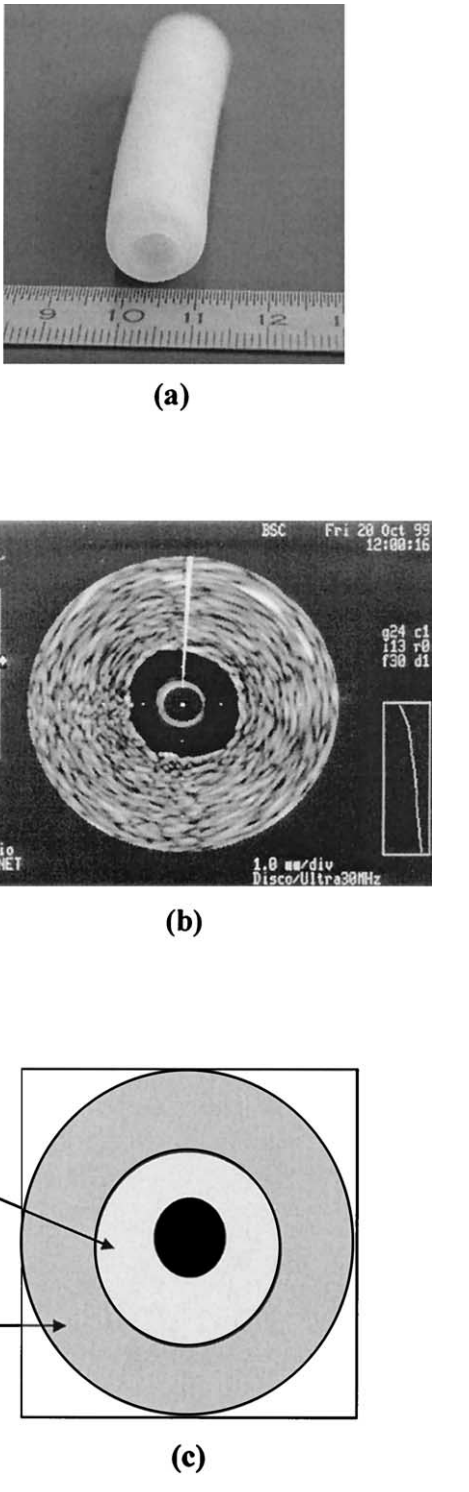

Fig. 4. Description of the two-layer intravascular cryogel phantom. The geometrical characteristics of this phantom are a 3 mm lumen diameter, a 5 mm wall thickness and a 60 mm length. The inner layer, the softer one, has been subjected to one freeze-thaw cycle, whereas the hard layer has been obtained by three freeze thaw cycles. (a) Photograph of the phantom; (b) B-mode image of the phantom; and (c) scheme of a phantom cross-section.

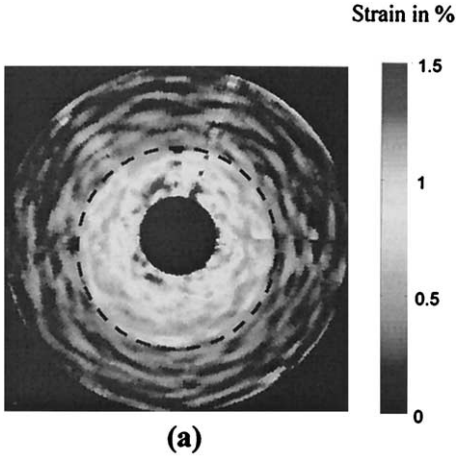

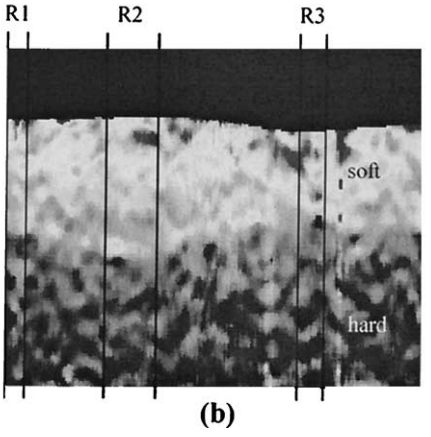

Fig. 5. Resulting elastograms from the two-layer intravascular cryogel phantom. (a) Elastogram in Cartesian representation computed with a 0.25 mm window length and 80% overlap; and (b) elastogram in polar coordinates.

from an increase of the water pressure inside the lumen, resulting in a mean inner radius raise of 6.3%. Reported strains are in the range of 0–6%.

It clearly seems that, whereas the phantom is mechanically homogeneous, the elastogram presents a decrease in the strain profile as a function of the distance from the lumen. Figure 3c displays a mean strain profile, computed over a region of 133 lines, where the phantom wall is at a constant distance from the transducer and, therefore, where signals are in correspondence. The mean strain decreases from 4.5% to 1% over only a few mm. Such a result meets the theoretical framework, which states that the propagation of the stress depends not only on the mechanical properties of the medium and on the boundary conditions, but also on the geometrical features of the medium and of load applications. Taking the particular case of hollow cylinders subjected to an inner pressure, even when isotropic and homogeneous, the propagation of the stress is not uniform, but decreases in amplitude across the thickness of the wall. This decay is a function of the radius, more precisely proportional to $1/r^2$ (eqn 6 Hearn 1997).

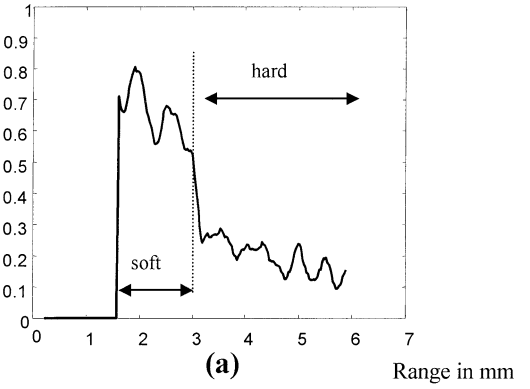

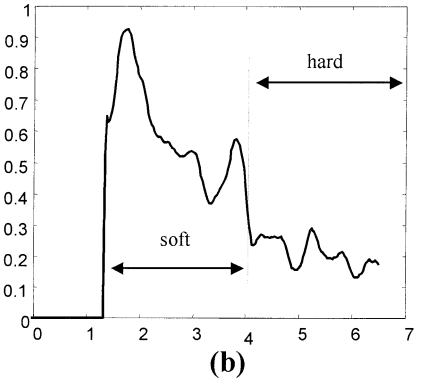

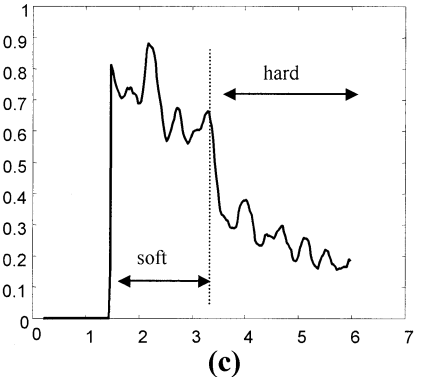

Fig. 6. Mean strain profiles display from the two-layer intravascular cryogel phantom elastogram. (a), (b) and (c) Respectively, three mean strain profiles computed over the regions R1, R2 and R3. Although a significant decrease of the magnitude of the stress exists across the wall thickness of the phantom, the two layers are well-distinguished, with a well-defined boundary.

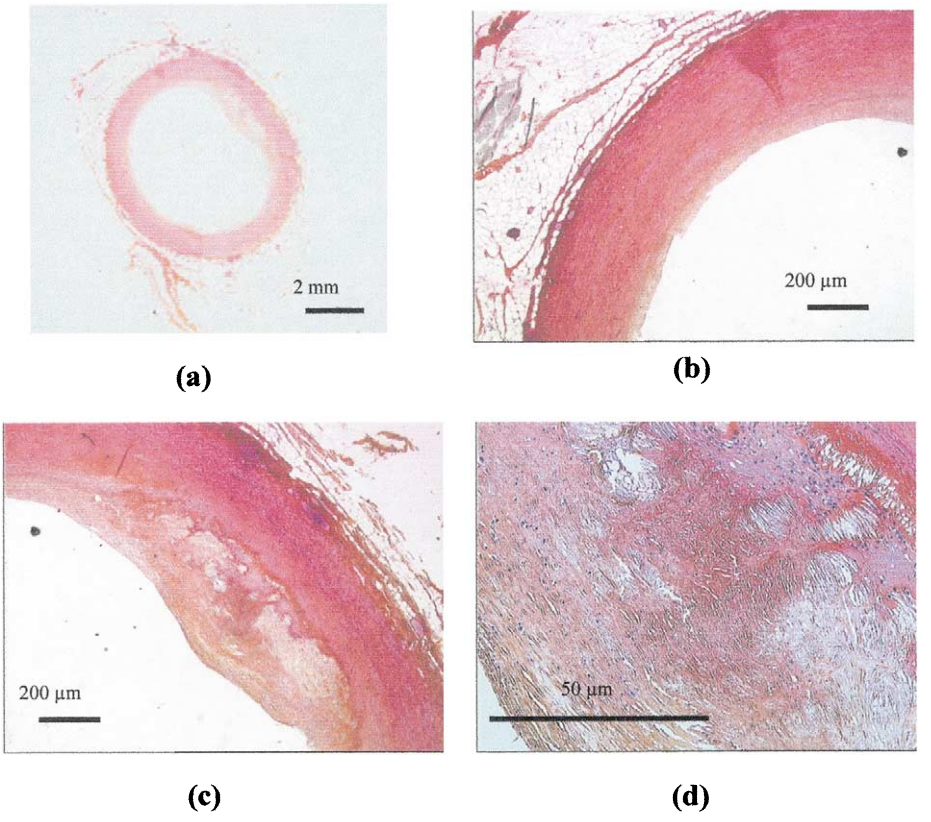

Fig. 7. Characteristics of the carotid artery. (a) Histological section of the carotid artery presenting a very thin plaque at 2 o'clock. (b) Visualisation of an healthy sector. (c) Visualisation of the plaque. (d) Colouration with saffron hematoxylin-eosin revealing the presence of cholesterol crystals and inflammatory cells within the plaque.

$$\sigma_r = \frac{a^2\, b^2\, (P_0 - P_i)}{b^2 - a^2} \cdot \frac{1}{r^2} + \frac{P_i a^2 - P_0 b^2}{b^2 - a^2} \qquad (6)$$

with σ_r = radial stress; r = radius; a = inner radius of the phantom; b = outer radius; P_i = inner pressure; and P_o = the outer pressure.

This phenomenon is clearly observed on the elastogram. For comparison, a curve in A/r^2 is also displayed (dashed line), matching perfectly the observed strain profile. It has to be pointed out that the visualisation of the phenomenon is amplified by the fact that the phantom we use is thick compared with arterial dimensions. This has been voluntarily performed to investigate the way the stress propagates within phantom walls, for further elastogram interpretations. However, owing to the thinness of arterial walls, the decrease of the stress will not be sufficient to prevent the discrimination of the different mechanical regions. This point is illustrated in the following section.

Results on two-layer phantom

The second experiment was performed with a two-layer phantom whose dimensions approximate to the ones of the arterial structure, a 3-mm lumen diameter, a 5-mm wall thickness and a 60-mm length (Fig. 4a; it has to be pointed out that, for building procedure reasons, the layers (wall-thickness/lumen-diameter ratio of 1.6) are much thicker than healthy arterial walls (ratio of 0.1). However, in the case of diseased arteries, a similar ratio can be reached. The inner layer is the softer one and measures 2.5 mm thick, and the hard one 2.5 mm as well. The soft layer has been subjected to only one freeze-thaw cycle, whereas the harder one has suffered from three cycles. The two layers are not concentric, but slightly off centre (Fig. 4c). No acoustical difference has been introduced between the two layers (Fig. 4b); their echogenicity results from the addition of acoustical particles for a concentration of 1%.

The strain estimation was performed with a 0.25-mm window length with 80% overlap. A 5×5 median filtering was applied to the estimates to reduce noise. The strain distribution results from an increase of the inner pressure, inducing a mean inner radius increase of 1.2%. The resulting elastogram is displayed in Cartesian (Fig. 5a) as well as in polar coordinates (Fig. 5b), the polar representation allowing a better visualisation of the

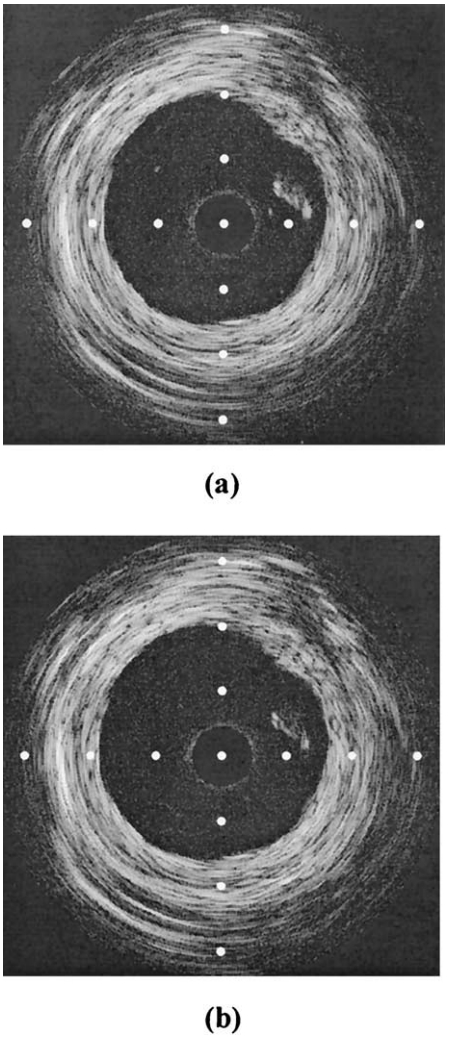

Fig. 8. Echograms of the carotid artery from (a) the initial and (b) final pressure levels, resulting in a maximal mean inner radius raise of 2.6%.

boundary between the two media. Reported strains are in the range 0–1.5%. Three mean strain profiles are also displayed (Fig. 6a–c). Because the two layers are not concentric, the boundary between them, in the polar representation, is not a straight line. To average corresponding information, the strain profile was computed over regions where signals are at a constant distance from the transducer. The profile 1 results from an average over a region of 12 lines, the profile 2 from an average over 33 lines, and the profile 3 from an average over 17 lines (see in Fig. 3e and f). From this different information, we can notice that the deformation over a layer decreases, affected by the heterogeneous character of the stress field. However, the two layers are discriminated with a well-defined boundary. The mean strain over the softer layer is estimated to 0.75% and to 0.25% over the harder layer. The strain ratio of three between the two layers matches data reported by Chu and Rutt (1997), about the PVA-C stress–strain relationship as a function of the number of freeze-thaw cycles. Effectively, a strain ratio between two and four is expected for two layers of PVA-C subjected to one and three freeze-thaw cycles.

In vitro results on a carotid artery

The ultimate goal of intravascular elastography is to characterise atherosclerotic plaque morphology and mechanical behaviour. Previous results performed on test objects have shown the potentiality of our strain estimation method to differentiate regions with different mechanical properties. While phantoms remain ideal test objects, they do not replace biological material. Performing experiments with arterial tissues seems to be an essential and indispensable step. For these reasons, we present, in this study, results obtained with a human excised postmortem carotid artery, exhibiting a very thin plaque at 2 o'clock (Fig. 7a). From the histological section, we can observe that the atherosclerotic plaque is a very limited region (Fig. 7c) and that the intima layer, except over this confined sector, presents healthy properties (Fig. 7b). The coloration with saffron haematoxylin-eosin reveals that the plaque contains cholesterol crystals and inflammatory cells (Fig 7d). Echograms (Fig. 8a and b) and elastograms displayed with adapted colour scales (Fig. 9a–d), were obtained for four consecutive increasing physiologic fluid pressure levels, resulting, respectively, in a mean inner radius increase of 0.75%, 1.2%, 1.6% and 2.6%. Elastograms were computed by using a 0.25-mm window length with 90% overlap. A 5×5 median filtering was applied to the estimates to reduce noise.

We can observe that, whereas the plaque reveals very low echo intensity differences in the echogram, it is clearly brought out in the different elastograms. The area of the harder region is effectively very well correlated with the plaque size, put in relief by the histological sections. The strain over the diseased region is significantly lower than that over the safe regions. As an example, in the elastogram (Fig. 9d), the deformation over the diseased region is less than 0.5%, whereas it is clearly more than 1.2% over the safe sector. Moreover, we can observe, on elastograms displayed with a unique common colour scale, that the strain difference between regions is all the more pronounced when the stress is high.

Finally, it has to be pointed out that the estimated strain values reach 3.5%, showing the potentiality of our strain estimation method for estimating higher strains.

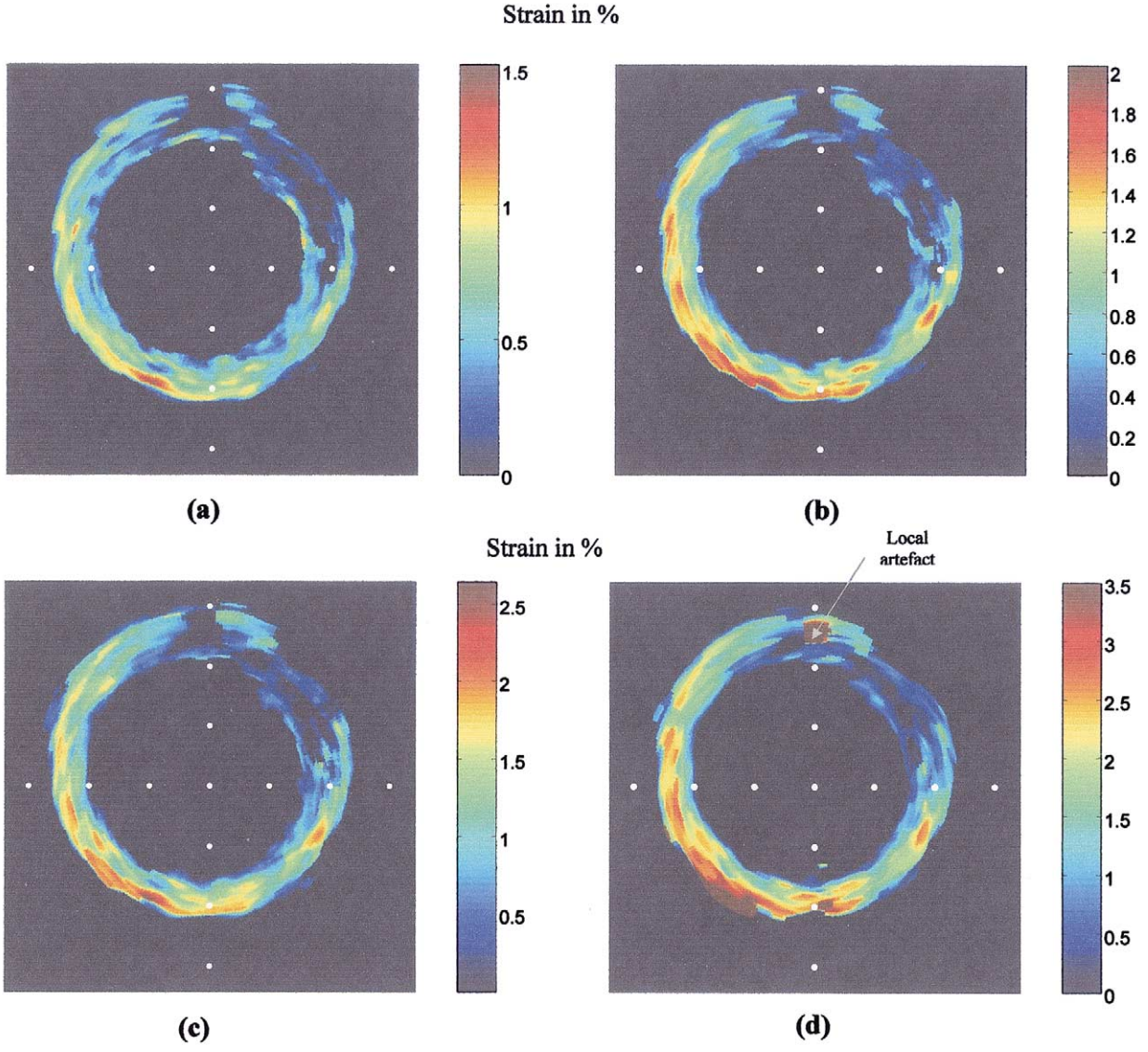

Fig. 9. Elastograms of the carotid artery. (a), (b), (c) and (d). Corresponding elastograms, displayed with adapted colour scales, and computed with a 0.25 mm window length and 90% overlap for an increase of the pressure level resulting in an inner radius increase of, respectively, 0.75%, 1.2%, 1.6% and 2.6%. The scale is given by markers distant of 1 mm. The indicated local artefact is induced by a high signal decorrelation. Whereas the plaque exhibits no acoustical difference with the healthy arterial wall, elastograms show that the diseased region is significantly harder than the surrounding safe tissue, allowing a precise visualisation of the diseased area.

CONCLUSIONS AND DISCUSSION

The study presented in this paper is a first approach for the application, in the intravascular case, of the strain estimation method we recently developed. This method has been proved to be accurate over a wider range of strains compared to commonly used gradient-based methods, making it very interesting for investigating heterogeneous media, like atherosclerotic arteries. For this investigation of feasibility, preliminary experiments were performed with original vessel-mimicking cryogel intravascular phantoms, as well as with a human fresh excised atherosclerotic carotid artery, subjected to a higher deformation.

Phantom elastograms have pointed out the potentiality of our strain estimation method to discriminate regions with different mechanical properties, although they exhibit no acoustical difference. A decrease of the strain is observed along the radial direction, due to the cylindrical geometry of the artery and loading conditions. However, the stress heterogeneity does not prevent the two layers from being discriminated with a well-defined bound-

ary, and does not significantly corrupt arterial wall investigation, because the latter are very thin structures.

On arterial elastograms, strain distributions for four consecutive increasing pressure levels are represented. We can observe that, in correlation with the histological sections, the diseased region seems to be significantly harder than the surrounding healthy tissue. A strain distribution within a wider range (0–3.5%), compared to reported results using classical gradient-based methods, allows a good visualisation of the deformation difference between the different regions and, therefore, a good discrimination between healthy and diseased sectors.

The information brought by elastography is thus complementary to ultrasound imaging and could provide useful indication on the nature of the plaque for a better diagnosis of atherosclerosis. Our future research efforts will concentrate on pursuing *in vitro* arterial experiments to study the reproducibility of this imaging technique and on studying its application in the *in vivo* conditions. This application will require preprocessing methods to compensate for motions introduced by the acquisition conditions. During the experiments we performed, the probe was fixed approximately at the centre of the phantom or artery lumen and parallel to its axis. But, in examination conditions, the probe is not going to be fixed, but will move with the variation of the blood pressure and the cardiac motion. Even when synchronised with the electrocardiogram, the acquisition will not provide images in correspondence. A preliminary image registration will be a fundamental step. Moreover, in clinical conditions, the probe is neither in the centre of the arterial lumen nor parallel to the arterial axis, but will be off-centred and with an angulation which can reach 30°. This relative position of the transducer with respect to the medium under investigation results in geometrical distortions on the ultrasound image, inappropriate for a further strain estimation. Such experimental conditions will require a preliminary processing to compensate for motions and distortions, before performing an elastographic study.

Acknowledgements—The authors would like to thank Mr. N. Rognin for his active participation during experiments and data acquisition, as well as Mr. A. Tabib for providing the carotid artery.

REFERENCES

Alam KS, Ophir J. Reduction of signal decorrelation from mechanical compression of tissues by temporal stretching: Applications to elastography. Ultrasound Med Biol 1997;23:95–105.

Alam KS, Ophir J, Konofagou EE. An adaptive strain estimator for elastography. IEEE Trans Ultrason, Ferroelec, Freq Contr 1998;45: 461–472.

Brusseau E, Perrey C, Delachartre P, et al. Axial strain imaging using a local estimation of the scaling factor from RF ultrasound signals. Ultrason Imaging 2000a;22:95–107.

Brusseau E, Delachartre P, Vray D. Axial strain imaging of vessel mimicking cryogel phantoms. IEEE Ultrasonics Symposium, Puerto-Rico, October 22–25, 2000b

Céspedes I. Elastography: Imaging biological tissue elasticity. PhD dissertation, Speciality: Electrical engineering, Houston, 1993, 287 p.

Chaturvedi P, Insana MF, Hall TJ. 2-D Companding for noise reduction in strain imaging. IEEE Trans Ultrason, Ferroelectr, Freq Contr 1998;45:179–191.

Chu KC, Rutt BK. Polyvinyl alcohol cryogel: An ideal phantom material for MR studies of arterial flow and elasticity. Magn Reson Med 1997;37:314–319.

Davies MJ, Thomas AC. Plaque fissuring—the cause of acute myocardial infarction, sudden ischaemic death, and crescendo angina. Br Heart J 1985;53:363–373.

De Korte CL. Intravascular ultrasound elastography. Thése Universitè Erasmus de Rotterdam, 1999, 180 p.

De Korte CL, Céspedes I, Van der Steen AFW, Lancée CT. Intravascular elasticity imaging using ultrasound: Feasibility studies in phantoms. Ultrasound Med Biol 1997a;23:735–746.

De Korte CL, Van der Steen AFW, Céspedes I, Pasterkamp G. Intravascular elastography of human femoral arteries: An in vitro study. IEEE Ultrasonics Symposium, Toronto, 1997b;2:1075–1078.

Di Mario C, Gorge G, Peters R, et al. Clinical applications and image interpretation in intracoronary ultrasound. Eur Heart J 1998;19: 207–229.

Emelianov SY, Lubinski MA, Weitzel WF, et al. Elasticity imaging for early detection of renal pathology. Ultrasound Med Biol 1995;21: 871–883.

Finet G, Maurincomme E, Tabib A, et al. Artifacts in intravascular ultrasound imaging: Analyses and implications. Ultrasound Med Biol 1993;19:533–547.

Finet G, Moll T, Tabib A, et al. Analyse de la performance diagnostique de l'échographie endovasculaire par les courbes ROC. Arch Maladies Coeur Vaisseaux 1997;90:59–66.

Fisher A, Gustein DE, Fayad ZA, Fuster V. Predicting plaque rupture: Enhancing diagnosis and clinical decision-making in coronary artery disease. Vasc Med 2000;5:163–172.

Fung YC. Biomechanical properties of living tissues. 2nd ed. New York: Springer Verlag, 1993:568 p.

Gao L, Parker KJ, Lerner RM, Levinson SF. Imaging of the elastic properties of tissue—a review. Ultrasound Med Biol 1996;22:959–977.

Gussenhoven EJ, Essed CE, Lancée CT, et al. Arterial wall characteristics determined by intravascular ultrasound imaging: An in vitro study. J Am Coll Cardiol 1997;14:947–952.

Hall TJ, Bilgen M, Insana MF, Krouskop TA. Phantom materials for elastography. IEEE Trans Ultrason, ferroelectr, Freq Contr 1997; 44:1355–1364.

Hearn EJ. Mechanics of materials: An introduction to the mechanics of elastic and plastic deformation of solids and structural materials. 3rd edition. United Kingdom: Heinemann, 1997:456 p.

Hein A, O'Brien WJ. Current time-domain methods for assessing tissue motion by analysis from reflected ultrasound echoes—A review. IEEE Trans Ultrason, Ferroelectr, Freq Contr 1993;40:84–102.

Hoeks APG, Brands PJ, Smeets FAM, Reneman RS. Assessment of the distensibility of superficial arteries. Ultrasound Med Biol 1990;16: 121–128.

Kallel F. Propriétés élastiques des tissus mous à partir de l'analyse des changements spatio temporels dans les signaux ultrasonores. PhD thesis, Ecole Polytechnique de Montreal, Canada, 1995, 142 p.

Konofagou EE, Ophir J. A new elastographic method for estimation and imaging of lateral displacement, lateral strains, corrected axial strains and Poisson's ratio in tissues. Ultrasound Med Biol 1998; 24:1183–1199.

Lee RT, Grodzinsky AJ, Frank EH, Kamm RD, Schoen FJ. Structure-dependent dynamic mechanical behavior of fibrous caps from human atherosclerotic plaques. Circulation 1991;83:1764–1770.

Lendon CL, Davies MJ, Born GV, Richardson PD. Atherosclerotic plaque caps are locally weakened when macrophage density is increased. Atherosclerosis 1991;87:87–90.

Lorenz A, Sommerfeld H-J, Garcia-Schürmann M, et al. A new system for the acquisition of ultrasonic multicompression strain images of

the human prostate in vivo. IEEE Trans Ultrason, Ferroelectr Freq Contr 1999;46:1147–1154.

Lubinski MA, Emelianov SY, O'Donnell M. Speckle tracking methods for ultrasonic elasticity imaging using short-time correlation. IEEE Trans Ultrason, Ferroelectr, Freq Contr 1999;46:82–96.

Nissen SE, Ziada K, Tuczu EM. Detection of atherosclerosis and identification of vulnerable plaque: potential role of intravascular ultrasound. In: Fuster V, ed. The vulnerable atherosclerotic plaque: understanding, identification and modification. New York: Futura Publishing Company, Inc.; 1999;87–109.

O'Donnell M, Skovoroda AR, Shapo BM, Emelianov SY. Internal displacement and strain imaging using ultrasonic speckle tracking. IEEE Trans Ultrason, Ferroelectr, Freq Contr 1994;41:314–324.

Ophir J, Céspedes I, Ponnekanti H, Yazdi Y, Li X. Elastography: A quantitative method for imaging the elasticity of biological tissues. Ultrason Imaging 1991;13:111–134.

Palmer ND, Northridge D, Lessels A, McDicken WN, Fox KAA. In vitro analysis of coronary atheromatous lesions by intravascular ultrasound. Eur Heart J 1999;20:1701–1706.

Richardson PD, Davies MJ, Born GVR. Influence of plaque configuration and stress distribution on fissuring of coronary atherosclerotic plaque. Lancet 1989;2:941–944.

Surry KJM, Blake CC, Chu KC, et al. Polyvinyl alcohol phantoms for use in MR and US imaging. Med Phys 1998;25:1082–1084.

Xu X-L, Tewfik AH, Greenleaf JF. Time delay estimation using wavelet pulsed-wave ultrasound. Ann Biomed Engin 1995;23:612–621.

Zaman AG, Helft G, Worthley SG, Badimon JJ. The role of plaque rupture in coronary artery disease. Atherosclerosis 2000;149:251–266.